Feedback control of microbubble cavitation for ultrasound-mediated blood–brain barrier disruption in non-human primates under magnetic resonance guidance

Hermes Kamimura, Julien Flament, Julien Valette, Andrea Cafarelli, Romina Aron Badin, Philippe Hantraye, Benoit Larrat

▶ **To cite this version:**

HAL Id: cea-02043269
https://cea.hal.science/cea-02043269

Submitted on 20 Feb 2019
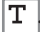
Page Proof Instructions and Queries

Journal Title: Journal of Cerebral Blood Flow & Metabolism (JCB)

Article Number: 753514

Thank you for choosing to publish with us. This is your final opportunity to ensure your article will be accurate at publication. Please review your proof carefully and respond to the queries using the circled tools in the image below, which are available **by clicking "Comment"** from the right-side menu in Adobe Reader DC.*

Please use *only* the tools circled in the image, as edits via other tools/methods can be lost during file conversion. For comments, questions, or formatting requests, please use ⊤. Please do *not* use comment bubbles/sticky notes 💬.

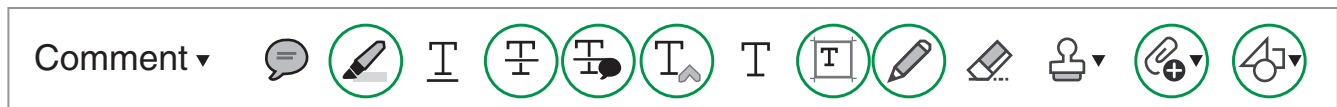Comment ▾   💬 ✏️ ⊤ ⊤̄ ⊤̄💬 ⊤ᴧ ⊤ T ✏️ 🧽 📑▾ 📎▾ 🎨▾

*If you do not see these tools, please ensure you have opened this file with Adobe Reader DC, available for free at get.adobe.com/reader or by going to Help > Check for Updates within other versions of Reader. For more detailed instructions, please see us.sagepub.com/ReaderXProofs.

No.	Query
	Please confirm that all author information, including names, affiliations, sequence, and contact details, is correct.
	Please review the entire document for typographical errors, mathematical errors, and any other necessary corrections; check headings, tables, and figures.
	Please confirm that the Funding and Conflict of Interest statements are accurate.
	Please ensure that you have obtained and enclosed all necessary permissions for the reproduction of artistic works, (e.g. illustrations, photographs, charts, maps, other visual material, etc.) not owned by yourself. Please refer to your publishing agreement for further information.
	Please note that this proof represents your final opportunity to review your article prior to publication, so please do send all of your changes now.
AQ: 1	Plesae provide the page range in Ref. 34.
AQ: 2	Please provide the location and details of the publisher in Ref. 41.

Feedback control of microbubble cavitation for ultrasound-mediated blood–brain barrier disruption in non-human primates under magnetic resonance guidance

Hermes AS Kamimura[1,2], Julien Flament[1,3], Julien Valette[1],
Andrea Cafarelli[2,4], Romina Aron Badin[1], Philippe Hantraye[1]
and Benoît Larrat[2]

Abstract

Focused ultrasound (FUS) in combination with microbubbles is capable of noninvasive, site-targeted delivery of drugs through the blood–brain barrier (BBB). Although acoustic parameters are reproducible in small animals, their control remains challenging in primates due to skull heterogeneity. This study describes a 7-T magnetic resonance (MR)-guided FUS system designed for BBB disruption in non-human primates with a robust feedback control based on passive cavitation detection (PCD). Contrast enhanced T_1-weighted MR images confirmed the BBB opening in monkeys soni-cated during 2 min with 500-kHz frequency, pulse length of 10 ms, and pulse repetition frequency of 5 Hz. The safe acoustic pressure range from 185 ± 22 kPa to 266 ± 4 kPa was estimated from combining data from the acoustic beam profile with the BBB opening and hemorrhage profiles obtained from MR images. A maximum BBB permeabilization was observed at 30 min after sonication with a relative contrast enhancement of $67\% \pm 15\%$ (in comparison to found in muscles). The feedback control based on PCD using relative spectra was shown to be robust, allowing comparisons across animals and experimental sessions. Finally, we also demonstrated that PCD can test acoustic coupling conditions, which improves the efficacy and safety of ultrasound transmission into the brain.

Introduction

The pharmacological treatment of neurodegenerative diseases, brain tumors and psychiatric illness is limited by the poor penetration of drug molecules into the central nervous system (CNS) imposed by the blood–brain barrier (BBB).[1] The selective permeability of the BBB is necessary to maintain the microenvironment adequate for brain cells to function. However, it prevents achieving therapeutic concentrations of potentially effective lipid-soluble drugs due to efflux transporters,[2] as well as, large, water soluble compounds due to transmembrane passive transport blocking.[3–5] Recently, focused ultrasound (FUS) in combination with intravenous injection of microbubbles has been demonstrated

[1]Molecular Imaging Research Center, Institut de Biologie François Jacob, Commissariat à l'énergie atomique et aux énergies alternatives (CEA), Fontenay-aux-Roses, France
[2]NeuroSpin, Institut des Sciences du Vivant Frédéric Joliot, Commissariat à L'énergie Atomique et aux Énergies Alternatives (CEA), Gif-sur-Yvette, France
[3]Institut National de la Santé et de la Recherche Médicale (Inserm), Fontenay-aux-Roses, France
[4]The BioRobotics Institute, Scuola Superiore Sant'Anna, Pontedera, Italy

Corresponding author:
Benoît Larrat, Centre CEA Saclay-Neurospin Bat 145, Gif-sur-Yvette RD306 – 91191, France.
Email: benoit.larrat@cea.fr

capable of non-invasively, transiently, and locally increasing the BBB permeability[6] through transcytosis and tight junction disruption accompanied by inhibition of active transport proteins in the brain endothelial cells.[7–9] The BBB disruption achieved with FUS in rodents allows reversible extravasation of molecules to the parenchyma with varied hydrodynamic diameters (up to 65 nm[10]). The BBB disruption may last from hours[10] to days[11] depending on the experimental protocol and the severity of disruption achieved. A recent study reported sterile inflammatory responses in the parenchyma that lasted for 24 h showing the need of a reliable method to ensure safety and reduce harmful bio-effects before this technique can be clinically translated.[12] Yet, this approach holds promising potential for the treatment of brain tumors, Parkinson's disease, and Alzheimer's disease demonstrated in rodents with the increase of the BBB permeability for variable-sized molecules such as antibody-based anticancer agents,[13–15] anti-amyloid antibodies,[13,16,17] brain-derived neurotrophic factor,[18,19] adeno-associated viruses,[20,21] and stem cells.[22]

The presence of the skull is the main challenge for the application of the FUS-mediated BBB disruption in humans. The high attenuation and scattering caused by the skull generates focus aberration and other undesired effects, such as standing waves[23] that can be partly overcome by sweeping frequencies.[24] Moreover, the mechanisms underlying this technique are not fully understood and its long-term consequences still require further studies. Large animal models, more specifically non-human primates (NHPs), are more adequate for studying such effects, because of the skull heterogeneity (variable thickness and complex internal microstructures[25]) and brain size, the similarity in anatomical and functional complexity of structures to humans, and the potential to perform sophisticated behavioral and cognitive tests. A limited number of studies using NHP has been reported that have yielded essential information on the safety of repeated sonication sessions[26,27] was demonstrated, as well as the influence of anesthesia in the BBB opening volume[28] and the associated drug delivery efficiency regarding the heterogeneity of brain anatomy and vasculature.[29]

Current FUS systems employed for BBB disruption in NHP's and humans adopted low-frequency ranges (220 kHz[26] or 500 kHz[30]) or implantable devices[31,32] to overcome the skull effects. A clinical system primarily designed for thermal ablation of the brain has been used in NHPs with the advantage of also providing MRI guidance[33] – so-called magnetic resonance imaging-guided focused ultrasound (MRgFUS).[34,35] Although, clinical trials with FUS-mediated BBB disruption were launched, a robust real-time feedback method for controlling the acoustic pressure has not yet been achieved.

Due to late detectability of edema or hemorrhage in MRI, methods based on passive cavitation detection (PCD) have been the preferred method for real-time monitoring of the safety during ultrasound-mediated BBB opening. PCD uses a broadband ultrasound transducer to detect the ultrasound scattering during sonication. In the presence of microbubbles, the spectrum of the scattered signals present changes in intensity and frequency composition. Sharp increases of harmonics and ultra-harmonics were associated with safe BBB disruption, whereas the presence of broadband emissions was associated with brain tissue damage[36,37] and used as an endpoint criterion. Current real-time techniques based on PCD monitoring analyze ultra-harmonics,[38] sub-harmonics,[39] and full frequency bandwidth.[40] However, those methods do not monitor broadband emissions of collapsing microbubbles[38,39] or mask these emissions with harmonic components[40] (orders higher in magnitude) leading to sonication with non-optimized pressure levels. Moreover, sub-harmonic based feedback control[39] may not be reliable, since sub-harmonics are highly associated with transient cavitation events.[41] In addition to that, all these techniques make use of absolute spectrum giving rise to false positive detections. In the method employing ultra-harmonic cavitation as the main index for the feedback control,[38] other problems such as system technical errors, errors in targeting, and error in detection of ultra-harmonics forced the exclusion of data from the overall analysis. The absolute spectrum results from all ultrasound interactions in the media, including signals generated from inadequate acoustic coupling. Thus, actual microbubble emissions are hardly extracted from other sources of scattering (i.e. bubbles trapped in the water coupling tank).[38] The use of a relative spectrum has been presented as a reliable method for separating microbubble emissions from signals generated by other sources.[42] However, no real-time feedback control using relative spectrum for controlling the acoustic pressure has been described to date.

In this study, we report a high field (7T) MRgFUS system designed for NHP using relative PCD spectrum-based real-time feedback control as a tool for better understanding the FUS-mediated BBB disruption, developing drugs, and studying diseases. The system was designed to provide high-resolution anatomical images and to follow the diffusion of the contrast agent with improved time and spatial resolution. We present here a safe control of acoustic cavitation and a test of the acoustic coupling designed and validate for the first time in NHP.

Material and methods

In vivo experiments

All experiments were conducted in accordance with European (EU Directive 86/609), French regulations (French Act Rural Code R 214-87 to 126) and performed according to ARRIVE (Animal Research: Reporting In Vivo Experiments) guidelines for the care and use of laboratory animals. The animal facility was approved by local veterinarian authorities (Authorization no. B 92-032-02) and complies with Standards for Humane Care and Use of Laboratory Animals of the Office of Laboratory Animal Welfare (OLAW –#A5826-01). The experimental protocol was approved by the Ethics committee CEtEA n°44 and the Ministry of Research and Education (Authorization n° APAFIS#908-2015062410594279v2). Experiments were conducted in four male cynomolgus monkeys (*Macaca fascicularis*, age: four to six years, weight: 4.1–7.9 kg, supplied by Noveprim, Mauritius Island) initially sedated with a mixture of ketamine/xylazine (10:1 mg/kg) and maintained sedated with intravenous infusion of propofol during the whole experiment at a rate of 1 ml/kg/h. Topical anesthetic (lidocaine) was used during intubation and during placement in the stereotaxic frame's ear bars to minimize pain. The heart and respiratory rates were monitored throughout the experiment (Resp./2_CH IBP, SA Instruments Inc., NY, USA). A flexible heating pad (SA Instruments Inc., NY, USA) maintained the animal's temperature at 37°C.

Experimental setup

The mechanical parts were designed in-house and manufactured by companies according to the following guidelines. All parts were MR compatible (Figure S1). An annular array ultrasonic transducer (center frequency: 500 kHz, frequency bandwidth: 300 to 700 kHz, number of elements: 14, diameter: 7 cm, spherical focusing radius: 6 cm; Imasonic SAS, Voray sur l'Ognon, France) was designed with spherical shape and a hole in the center for the placement of a monitoring ultrasonic transducer (described in the following section, PCD). The transducer was fixed in a probe holder (M2E, Eaubonne, France) with a water circulation system that controlled for degassing and hydrostatic pressure. The probe holder presented a latex-based membrane for acoustic coupling of the transducer with the animal's head previously shaved and covered with degassed acoustic coupling gel. The probe holder was fixed in a two-dimensional stereotaxic frame (M2E, Eaubonne, France) where the animal was placed in sphinx position inside a 7-T horizontal MR imaging system (Varian-Agilent Technologies Inc., California, USA). A dedicated surface loop coil for monkey head (H 299 MHz, $\varnothing_{int} = 13.5$ cm; RAPID Biomedical GmbH, Rimpar, Germany) was placed between the transducer holder and the animal's head. The transducer was driven by an RF-amplifier (LabFUS, Image Guided Therapy, Bordeaux, France). After intravenous injection of microbubbles (dose: 0.30 mL/kg; SonoVue, Bracco Imaging S.p.A., Italy), local sonication was applied for 2 min with pressure ranging from 0.09 to 1.2 MPa (calibrated in free water), 500-kHz frequency, pulse repetition frequency of 5 Hz, and pulse length of 10 ms (5000 cycles or 5% duty cycle).

PCD

A planar mono-element ultrasonic transducer (center frequency: 1.53 MHz, frequency bandwidth: 58%, diameter: 4.5 mm; Imasonic SAS, Voray sur l'Ognon, France) positioned at the center of the therapeutic ultrasonic transducer was used to passively detect the ultrasonic waves backscattered by the animal's head and microbubbles. The signal detected by the PCD transducer was acquired by an oscilloscope (PicoScope 5242B, Pico Technology, Cambridgeshire, UK), which in turn was controlled and synchronized with the MRgFUS system by a software developed in Python (version 2.7.12, Python Software Foundation, Delaware, USA). The frequency components of the signal (sampled at 31.25 MHz) were quantified by computing the average and maximum values resulted from the fast Fourier transform (FFT) as described by Wu, et al.[43] The FFT calculation was optimized using the library pyFFTw.[44] Relative power spectra were obtained from the ratio of the total power spectrum (after microbubbles injection) and the power spectrum of the averaged baseline. The frequency components were calculated at bandwidths of $\Delta f_{sub} = 50$ kHz around the sub-harmonic ($f_{sub} = f/2 \pm \Delta f_{sub}$), $\Delta f_{harm} = 100$ kHz around the harmonics ($f_{harm} = n*f \pm \Delta f_{harm}$, with n = 2, 3, and 4), and $\Delta f_{ultra} = 50$ kHz around the ultra-harmonics ($f_{ultra} = m*f \pm \Delta f_{ultra}$, with m = 1.5, 2.5, 3.5, and 4.5). The stable cavitation dose (SCD) was determined as the sum of the root mean square (RMS) of the harmonic and ultra-harmonic frequency components. The inertial cavitation dose (ICD) was determined as the RMS of the broadband signal excluding the frequency bandwidths of the SCD.

PCD-based feedback control

The algorithm for controlling the acoustic pressure consisted of recording baseline spectra at different pressures before microbubble injection and obtaining the

ICD and SCD from the relative power spectrum (RPS) (Figure S2). RPS was defined as the ratio of the instantaneous signal power spectrum after microbubble injection and the correspondent baseline power spectrum.

$$RPS = \frac{S_P}{B_p} \tag{1}$$

where S_p is the power spectrum of the signal after microbubbles injection at certain acoustic pressure P, and B_P is the correspondent averaged baseline power spectrum at same acoustic pressure P. Averaged baseline spectra ($n = 5$) were obtained from acquisitions at acoustic pressures ranging from 90 to 1157 kPa with steps of 9 kPa (calibrated at focus in free water). Plots of the SCD and ICD at baseline were used to reveal inadequate acoustic coupling. Immediately after baseline acquisition, microbubbles were injected and the sonication was applied starting at 580 kPa and increasing gradually by 9 kPa until a defined SCD was reached or decreasing when ICD was detected. The ICD detection was performed for every pulse during the entire sonication period (2 min). A graphical user interface was built to embed all functions using Python TKinter.

Calibrations and in vitro tests

Calibrations were performed in a tank filled with degassed Mili-Q water (oxygen <10% or 0.80 mg/L at 22°C, Aqualyse Pro20 oximeter, Aqualabo Contrôle, France) with a hydrophone (HGL-0200, Onda Corp., Sunnyvale, CA, USA) fixed in a 3D positioning system (AcousticExplorer, Image Guided Therapy, Bordeaux, France). Three freshly excised skull specimens were degassed during 24 h and used for testing the attenuation of ultrasound. Three anatomical regions were evaluated for every specimen: (1) centered at hippocampus, (2) 2 cm caudal from 1, and (3) 2 cm rostral from 1 (Suppl. Figure S3). The skull was placed between the transducer and the hydrophone, with the skull approximately 3 cm away from the transducer and the hydrophone. The hydrophone was placed first at the focus of the transducer in free water, but after placing the skull specimens, the hydrophone was repositioned seeking for the highest signal (Figure S3b). The ultrasound focus shifts due to skull effects were calculated from the 3D coordinates of the hydrophone translation. The frequency bandwidth of the PCD transducer was acquired in the same fashion using a calibrated ultrasound source.

Magnetic resonance imaging

T_2-weighted images were acquired using a fast spin-echo sequence (TR = 4750 ms, TE = 20 ms, 450×450 µm2 in-plane resolution, 40 coronal slices, slice thickness = 1 mm) and were used to confirm the adequate acoustic coupling (absence of bubbles in the coupling gel, positioning of the water balloon over the ultrasound beam trajectory) and the target planning (expected focus position). Contrast enhanced 3D T_1-weighted images (TR = 2000 ms, TE = 3 ms, TI = 680 ms, resolution = $450 \times 450 \times 2000$ mm³, 64 coronal/sagittal slices) were used to evaluate the BBB disruption. T_1-weighted images acquired shortly before the sonication served as baseline to evaluate the contrast diffusion in the parenchyma. The gadolinium-based MRI contrast agent (dose: 0.20 mL/kg; DOTAREM®, Guerbet, Roissy, France) was injected following the PCD baseline acquisition immediately after microbubbles injection. The contrast agent dynamic was evaluated by acquiring T_1-weighted images every ~5 min during 40 min starting after the sonication was completed. The contrast enhancement due to gadolinium leakage was quantified in ImageJ in an elliptical region of interest (ROI) in the expected focus region. The absolute difference of the ROI's image brightness was calculated using the baseline MRI. The non-sonicated opposite brain hemisphere was used as an internal control ROI. The contrast enhancement in those regions was compared with the contrast enhancement in the muscles surrounding the animal's skull.

Results

Targeting planning and acoustic coupling evaluation

An example of targeting planning is shown in Figure 1(a) and (b) where the expected focus (focal width: 2.8 mm, axial length: 33.3 mm, and focal distance: 56.9 mm at 500 kHz; see Suppl. Figure S3 for more details of the calibration) was drawn on a T_2-weighted MR image based on the transducer geometry. The T_2-weighted MR images were also used to confirm adequate acoustic coupling. The optimal condition was when no bubbles were trapped between the water balloon and the animal's head in the FUS trajectory. Ultrasound pulse-echo signal was used to confirm the distance from the transducer to the skull with an estimation of the focus depth based on the ultrasound time-of-flight (Figure 1(c)).

In addition to T_2-weighted MR images, PCD was used to check the acoustic coupling quality. PCD baseline acquisitions before microbubble injection were performed for every acoustic pressure level used during feedback controlled sonication. Smooth growing of the harmonics and ultra-harmonics detection (H./U.H.) with no broadband emissions detected was observed when adequate acoustic coupling was

obtained (Figure 2(a) and (b)). On the other hand, inadequate coupling caused by bubbles trapped in the water balloon or acoustic coupling gel or non-sufficient degassing of water was indicated by broadband emissions and a sharp variation of the harmonics and ultra-harmonics emission (Figure 2(c) and (d)).
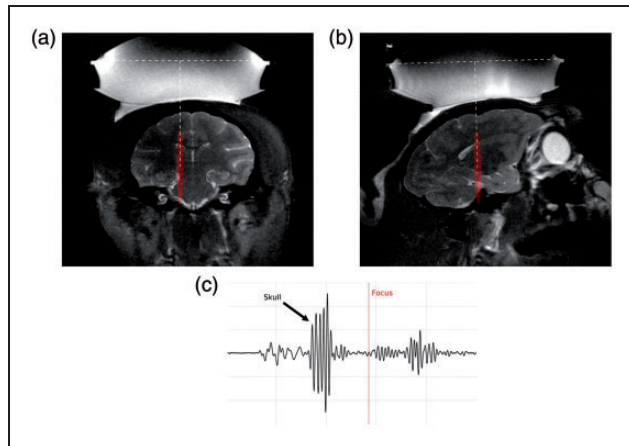

Figure 1. Target planning and verification of acoustic coupling. (a) Coronal and (b) sagittal slices at the expected focus region (in red) using T_2-weighted MR images (water balloon and coupling gel shown in hyper intense areas). (c) Pulse-echo ultrasound signal showing the skull reflection and estimated focus depth (red line) based on the ultrasound time-of-flight.

BBB opening and targeting confirmation

Gadolinium leakage observed in the contrast enhanced T_1-weighted MR images confirmed the BBB disruption (Figure 3). The average acoustic pressure attenuation based on calibrations with skull specimens varied from -5 dB in more rostral regions to -12 dB more caudal region (Suppl. Figure S3). The focal shifts caused by the skull due to aberration effects in vivo were 0.76 mm in the lateral direction and 3.64 mm in depth direction in the coronal slice and 1.44 mm in the lateral direction and 3.82 mm in depth direction in the sagittal slice. The shifts observed with skull specimens in a water tank varied from 1.40 to 2.10 mm (Suppl. Figure S4).

## BBB opening without feedback control of the acoustic pressure

Figure 4 presents a summary of experimental sessions without feedback control of the acoustic pressure. Lower pressures (697 kPa, calibrated in free water) resulted in mild or no BBB opening in sessions 1 and 2. Higher pressures (1.16 MPa, calibrated in free water) resulted in mild BBB opening in session 3, while the same pressure caused a permanent lesion in session 4 (Figure 4). The BBB opening intensity correlated with the harmonic cavitation doses, whereas broadband emission (ICD) and sub-harmonic components were
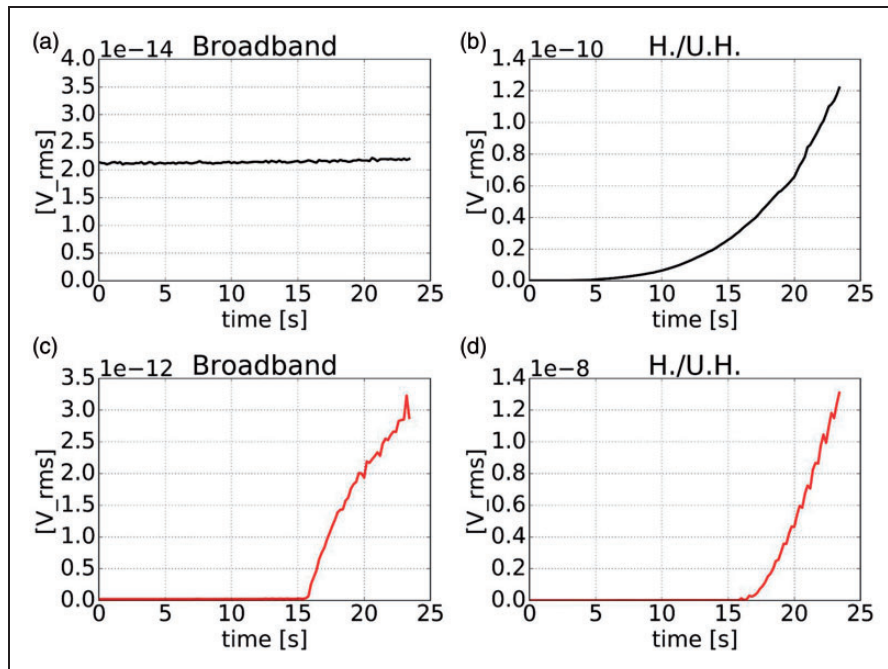
Figure 2. Acoustic emissions (in root mean square voltage, [V_rms]) on sham acquisitions (without microbubble injection) with linear increase of pressure with time. Representative broadband emission and harmonics and ultra-harmonics emissions (H./U.H.) acquired with adequate acoustic coupling (a, b) and inadequate acoustic coupling(c, d).
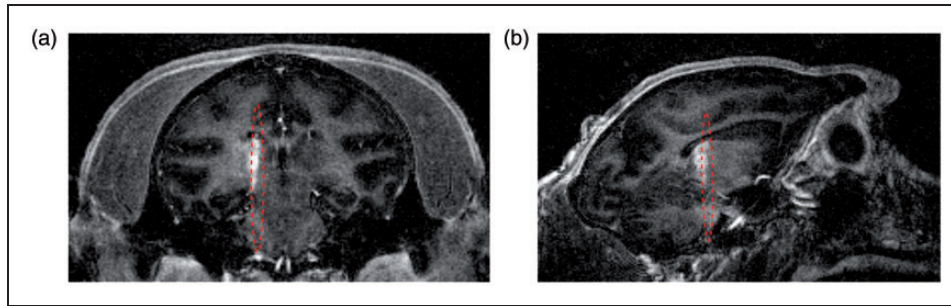
Figure 3. Contrast enhanced T_1-weighted MR images confirming the BBB opening within the targeted region (red) and beyond it, but with a shift in the (a) coronal slice of 0.76 mm lateral and 3.64 mm in depth and (b) 1.44 mm lateral and 3.82 mm in depth in the sagittal slice.
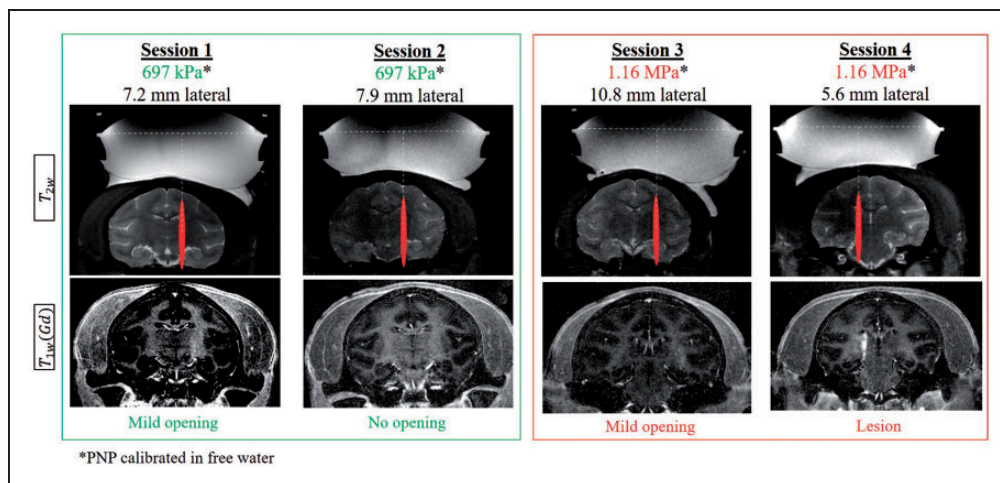
Figure 4. Summary of targeting and BBB opening using constant acoustic pressure (no feedback control). Representative coronal MR images showing targeting on T_2-weighted MR images (top) acquired prior to sonications and T_1-weighted contrast enhanced MR images acquired 30 min after sonication illustrating the presence (sessions 1, 3, 4) or absence (session 2) of BBB opening (bottom) using low (green) and high (red) acoustic pressures.

observed in the case that resulted in permanent lesion (Figure S5).

After 14 days, contrast enhanced T_1- and T_2-/T_2*-weighted MR images were acquired to evaluate the brain integrity after FUS-induced BBB opening. Blood extravasation was associated with a severe BBB disruption and high ICD in one case (session 4). In this case, both the BBB disruption and the associated damages were confined to the focus region, showing that, although with focus shifting, the surrounding tissue was preserved. Other cases presented a safe BBB disruption with no blood extravasation, associated with lower ICD (S1 and S3, Figure S5). The contrast enhanced T_1-weighted MR images acquired after 14 days presented no gadolinium extravasation in the parenchyma showing that the BBB was restored in all cases, including in the monkey with blood extravasation. Such extravasation did not give rise to any clinical signs or

changes in feeding and social behavior probably due to the localization of the lesion.

Estimation of safe acoustic pressure range

The use of a high field MR system allows the acquisition of images with high signal-to-noise ratio (SNR). Based on that, an effective and safe range of acoustic pressure was estimated from MR images of the animal that presented bleeding after sonication (session 4). The size of BBB opening was estimated from the contrast enhanced T_1-weighted MR image acquired within 5 min of sonication (Figure 5(a)). The size of the opening on the coronal slice was approximately 2.44 mm in width (lateral). T_2-weighted MR images acquired 14 days after sonication showed a reduction in the width of the hematoma to 1.45 mm (Figure 5(b)). Thus, out of all the brain tissue that presented BBB opening,
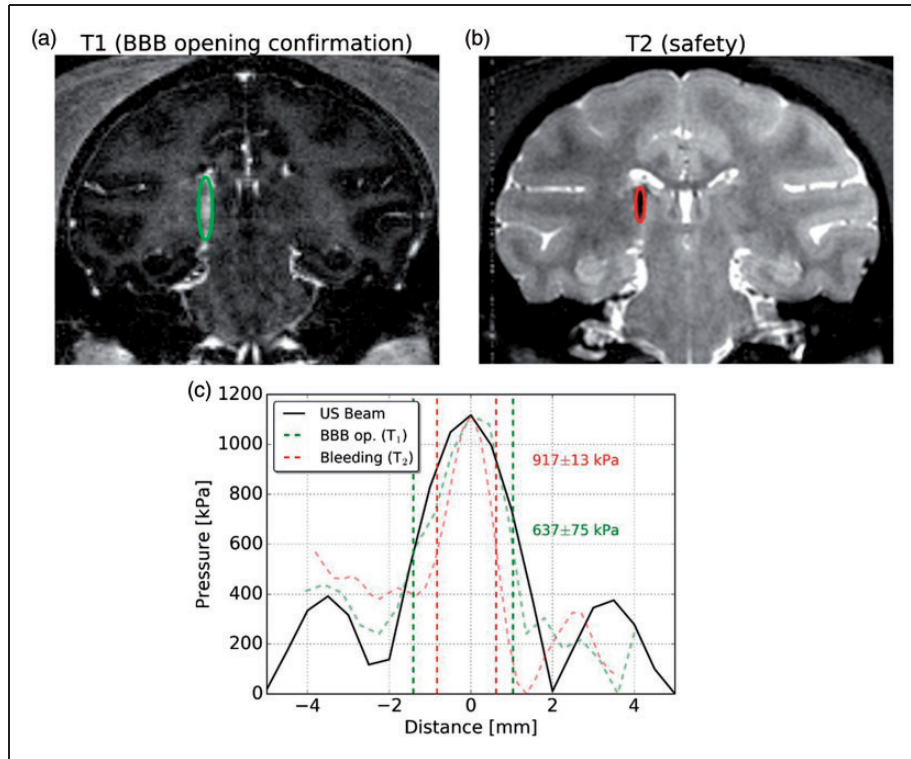
Figure 5. Estimation of the safe acoustic pressure range. (a) BBB opening area evaluated by contrast enhanced T_1-weighted MR images acquired 5 min after sonication and (b) hematoma detection after 14 days on T_2-weighted MR images, (c) ultrasound lateral beam profile in free water (black) plotted against the BBB opening lateral profile (green) and the hematoma lateral profile (red) extracted from (a) and (b), respectively.

bleeding was spatially limited to a region between ~~the~~ 1.45 and 2.44 mm of width. An estimation of the acoustic pressure that caused BBB opening was obtained by overlapping data from the BBB opening width profile with the acoustic beam profile (Figure 5(c)). On the other hand, the width profile of the resulting hematoma provided an estimation of the acoustic pressure that caused damage to the brain tissue (Figure 5(b)). Thus, the safe acoustic pressure range could be calculated by crossing this information as presented in Figure 5(c). The acoustic pressure range that resulted in safe BBB opening (without bleeding) ranged from 637 ± 75 kPa to 917 ± 13 kPa (in free water). The pressure range inside the brain was estimated from calibrations using skull specimens ($n = 3$). The minimum attenuation was found in the anterior part of the skull and was of 71%, resulting in an acoustic pressure range ~~of~~ 185 ± 22 kPa to 266 ± 4 kPa.

PCD-based feedback control of acoustic pressure

Harmonic and ultra-harmonic components were present after microbubble injection (Figure 6(b) and (c)). Harmonic components were always observed when BBB opening was successful (Figure 6(b)). Broadband and sub-harmonic components were strongly present when sonication resulted in a permanent lesion and they were not statistically significant in sessions that resulted in safe BBB opening (Figure 6(a) and (d)). Sessions performed with feedback control (green boxes) presented harmonic ~~C.D.~~ of intermediate values, higher than ~~C.D.~~ that resulted in mild BBB opening (black boxes) and lower than ~~C.D.~~ that resulted in a lesion (red box). The feedback control also succeeded in avoiding inertial C.D. and sub-harmonic ~~C.D.~~ It is important to notice that the boxplots represent the values throughout the sonication duration (120 s, Figure S6). Therefore, outliers in the sonication with feedback control are cavitation events detected when the acoustic pressure reached the maximum level. After cavitation events were detected, the algorithm rapidly converged the acoustic pressure to a safe level. As in previous studies with monkeys, ultra-harmonic ~~C.D. was~~ less detectable and not consistent in safe sessions, but ~~was~~ always lower than in the case that resulted in lesion. Performing the sonication inside the MRI provided a shielded environment making possible very low PCD acquisition ~~with no MR noise~~.

The BBB opening was evaluated by contrast-enhanced T_1-weighted images (Figure 7(a)). The contrast
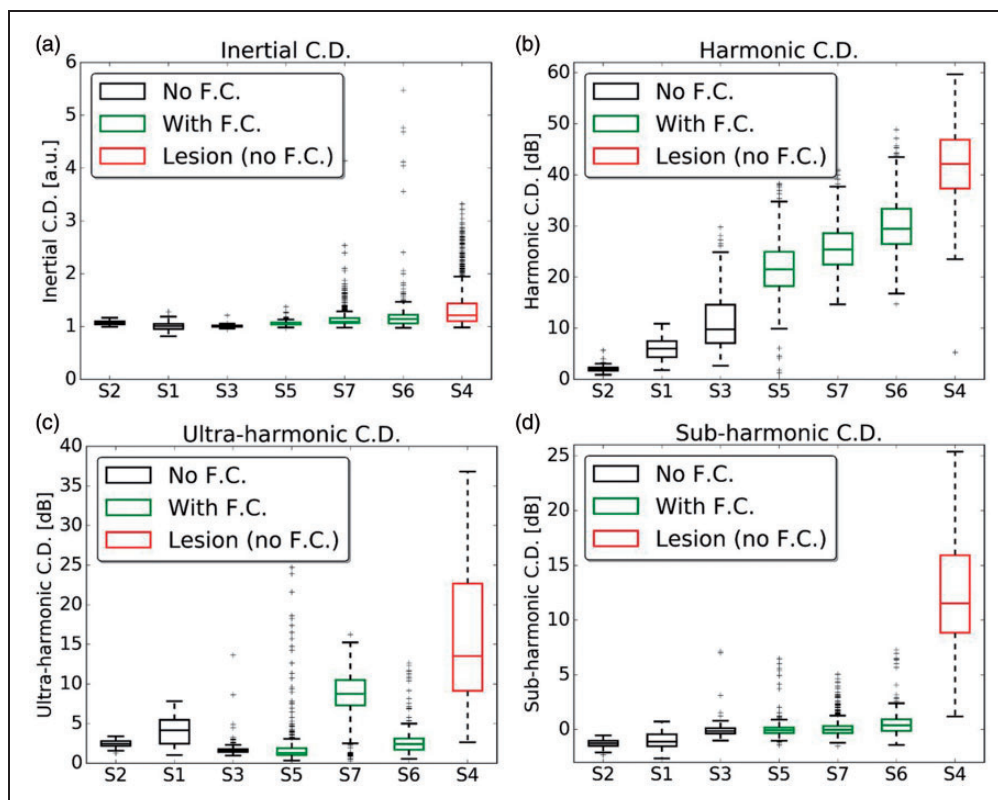
Figure 6. Boxplots representing relative inertial (a), harmonic (b), ultra-harmonic (c) and sub-harmonic (d) cavitation doses (C.D.) across all experimental sessions (S1–S7). Boxes in black and red are sessions with no feedback control (F.C.) of acoustic pressure, with red indicating the only session that resulted in a permanent brain lesion. Boxes in green are sessions with feedback control of acoustic pressure that resulted in safe BBB disruption. All cavitation doses are normalized to the baseline acquisition before microbubble injection. Time series of the cavitation doses are provided in the Suppl. Figure S6.

enhancement in the parenchyma was quantified by measuring the intensity of the images resulting from the subtraction of images acquired after sonication by the baseline images (T_1-weighted images acquired before sonication). Regions of interest (ROIs) were selected in the muscle (where gadolinium diffuses freely), the focal region (where sonication was performed in the parenchyma), and the contralateral focal region (where sonication was not performed in the parenchyma) (Figure 7(a)). The contrast enhancement found in the parenchymal ROIs was normalized to the contrast enhancement in muscle. On average, the sonicated region presented a maximum of $67\% \pm 15\%$ of the contrast enhancement found in muscle after 30 min of sonication for sessions using feedback control (S5–S7). The non-sonicated brain tissue (contralateral focal region) presented an average relative contrast enhancement of $11\% \pm 2\%$. The half-life of gadolinium in muscle was of approximately 40 min (exponential fit of the intensity I given by: $I = 0.765 * e^{-0.055*t} + 0.414$, see Suppl. Figure S7). In the session that resulted in permanent lesion (Figure 5), the maximum relative contrast enhancement was 2.25 times higher than in muscle.

Discussion

Preclinical trials with therapeutically relevant drugs validated in small animals have demonstrated the great potential of ultrasound-mediated BBB opening to treat brain tumors, neurodegenerative diseases and psychiatric disorders. However, the clinical translation of the technique requires scaling to larger animal models as well as providing reliable methods to ensure safety and reduce harmful bio-effects of the ultrasound. Real-time monitoring and image guidance will facilitate broadening the applications of ultrasound for drug delivery in the CNS.

In this study, we developed and validated in monkeys a system for ultrasound-mediated BBB opening with high-field MRI guidance and real-time acoustic-based feedback control. High-SNR MR images demonstrated successful BBB opening and allowed estimations of sonication parameters and its associated effects in the brain. We demonstrated that passive cavitation-based feedback control was capable of providing a reliable readout for moderating the BBB disruption while preserving non-targeted regions in the brain.
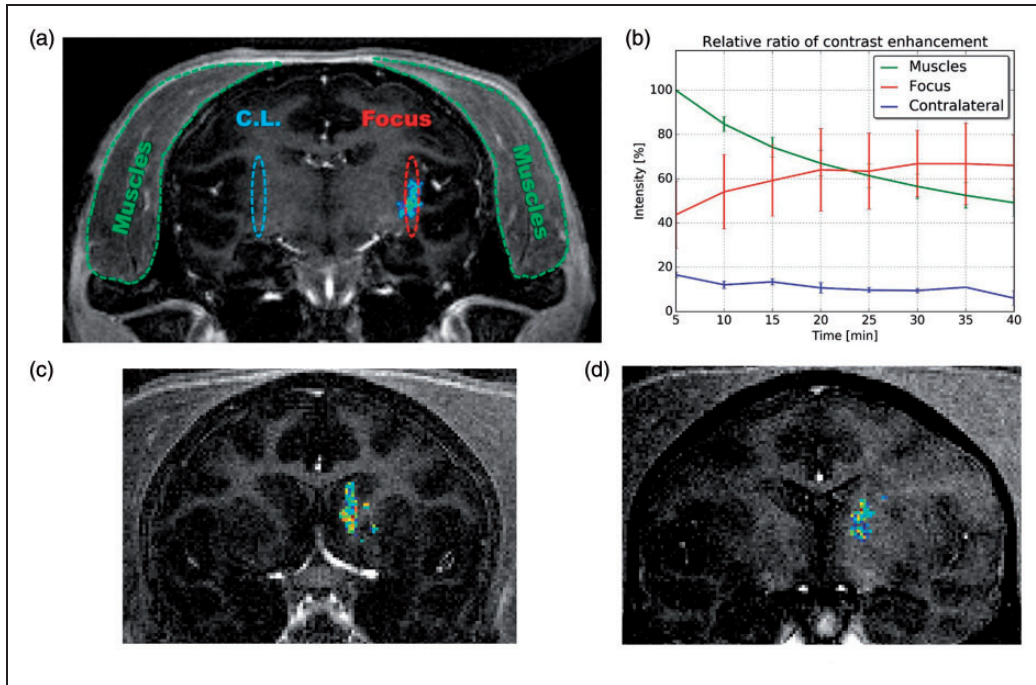
Figure 7. BBB opening obtained with feedback control. (a) Representative coronal T_1-weighted MR image after sonication over-lapped with the BBB opening area for session S7. The BBB opening region was segmented from the image resulting from the subtraction of the T_1-weighted MR images after (contrast image) and before sonication (baseline enhanced). (b) Estimated relative contrast enhancement found in sonicated, non-sonicated (contra-lateral), and muscles regions (percentage values in relation to the maximum intensity in muscles). (c) Representative coronal T_1-weighted MR image after sonication overlapped with the BBB opening area for session S5. (d) Representative coronal T_1-weighted MR image after sonication overlapped with the BBB opening area for session S6.

Broadband and sub-harmonic emissions were asso-ciated with lesions. Broadband emissions presented higher median values for sonication that resulted in lesion with an increase of outliers at higher acoustic pressure. The broadband emissions were the best index for the feedback control of the acoustic pressure to limit at the highest effective sonication, while avoid-ing harmful bubble activity. Inertial cavitation could arise from the muscles surrounding the NHP's head or originated from tolerable inertial activity in big ves-sels as described by a previous study.[29] Furthermore, as opposed to other study,[39] sub-harmonics had a lot higher activity in the case with lesion, which indicates these parameters should be intolerable in our system.

The targeting presented a shift of about 2 mm, which is in the order of the FUS beam width (2.7 mm). The focal shifts are more critical for finer focus, which are associated with higher ultrasound frequencies. In the case of maximum shift observed here, the BBB opening region was mostly inside the targeted area with a region of about 0.35 mm outside the intended focus. Focal shifts can be avoided by adjusting the transducer pos-ition with the aid of MR guidance in order to achieve a normal incidence angle. Moreover, even in the only severe BBB opening accompanied by tissue damage

in one monkey, the surrounding tissue showed normal perfusion/Gd penetration in the experiments performed 14 days after BBB opening suggesting that function was preserved in the tissue around the lesioned area.

The acoustic pressure range for safe BBB opening could be estimated by integrating data from the corres-ponding acoustic pressure on the acoustic beam profile obtained from calibrations with the size of BBB opening and the hematoma observed in the MRI. The estimation is not optimal to account for distorting effects, but calibrations using skull specimens at similar targeting provided a good approximation. This estima-tion highlights how critical is the acoustic pressure range to increase the BBB permeability, while avoiding severe damages in the brain. However, a subject-specific simulation based on CT- or MR-images together with a higher time-resolution MRI sequence have to be developed to allow a more precise evaluation of the minimum and maximum pressures inside the brain, as well as taking into account the pharmacokinetics of Gd. Yet, the high resolution and SNR of the current MRI sequence provided a good estimation of the location and size of BBB opening. Moreover, during sessions that resulted in safe BBB opening the hyper intensity observed in T_1-weighted MR images shows

an accumulation of gadolinium in the sonicated region, whereas at non-sonicated control and muscle regions, the relative contrast enhancement decreases with time.

The heterogeneity of the skull caused a high variability of the ultrasound transmission into the brain. According to the in vitro calibration using NHP skull specimens, higher acoustic pressure attenuation was found in anterior regions in comparison to posterior regions (Suppl. Figures S3 and S4). During in vivo ultrasound-mediated BBB opening sessions using constant pressure, lower acoustic pressures resulted in mild or no BBB opening, whereas higher pressures resulted in mild BBB opening or permanent lesion. The variability of the results demonstrates that constant acoustic pressure is not optimal for providing an effective and safe BBB opening.

Our experiments confirm that PCD detection of microbubble activity is a reliable readout for safe BBB opening. The SCD was a useful parameter to demonstrate effective microbubble activity. Excessive ICD and sub-harmonic frequency components were associated with permanent perfusion damages on MRI, thus serving as parameters to set a threshold of acoustic pressure for a safe sonication. This study was limited to evaluate radiologically visible damages such as hemorrhage and edema. Further studies are necessary to investigate the relationship between microbubble activity levels and tissue biochemical reactions such as fine indicators of inflammatory responses recently reported by Kovacs et al.[12]

The relative processing of PCD was presented by Arvanitis et al.[42] This method consists of acquiring baseline backscattered signals and processing relative spectrums by calculating the ratio of acquisitions after microbubble injection by the baseline signal (Suppl. Figure S8). The baseline acquisition is similar to the sham acquisition, except for the fact that a single level of acoustic pressure was adopted by Arvanitis et al. This method has been presented as an effective procedure for obtaining only microbubble activity while suppressing background noise and scattering. We adopted this method to remove the background noise of the full acoustic pressure range used in our feedback control. In our case, the backscattering signature for each acoustic pressure can be compared with the correspondent acquisition after microbubble injection. Other methods for feedback control of the acoustic pressure are based on monitoring the ultra-harmonic[38] and sub-harmonic amplitudes.[39] Although included in our system, these parameters are not the key readouts for acoustic pressure control. Instead, we use broadband emissions as a signature of the highest acoustic pressure level to obtain an effective and safe BBB opening. Previous studies have demonstrated that low levels of inertial cavitation are associated with

microbubble activity in large vessels that does not result in damages and are thus safe in NHP.[29] As a result, choosing an adequate tolerance for ICD allow a safe and effective control of BBB opening. Unlike other methods, relative emission monitoring guarantees feedback control throughout the whole sonication and provides a robust evaluation of the setup and the activity of bubbles, allowing comparison across different animals and setup conditions. Furthermore, our results corroborate that sub-harmonics are highly associated with transient cavitation events[41] and it was only present in the session that resulted in a permanent lesion. However, the system-independence of this result requires further studies. Although the relative spectra compensate for the lower sensitivity of the PCD out of the frequency bandwidth, additional studies using a PCD with frequency response at the sub-harmonic are necessary to conclude on the detectability of sub-harmonic in cases with safe microbubbles activity.

Furthermore, the method presented here provides spectra of the baseline acquisitions that illustrate the problems encountered with acoustic coupling. Testing acoustic coupling consists in running a sham experiment, that is to say recording broadband backscattered signals as a function of electrical power. The sham sonication includes all components of the experimental setup in feedback control mode except for the microbubble injection. Running sham sonications during sessions S5, S6 and S7 prior to sonications with microbubbles injection, we were able to acquire acoustic backscattering signatures of the setup revealing any bad coupling conditions like the presence of bubbles trapped in the gel or in the water balloon used to couple the transducer to the head of the NHP. Such signatures can be plotted in the frequency domain, where broadband emissions reveal the presence of bubbles, as well as variations in the amplitude of harmonic frequencies that show threshold nucleation due to no adequate degassing of water in the balloon. None of these effects are desired since they represent hallmarks of bad acoustic transmission to the organ of interest (degraded efficacy) and make it difficult to differentiate the activity of the injected microbubbles from bad coupling condition. To the best of our knowledge, no method for acoustic coupling checking was published so far. This innovation can be useful to all therapeutic applications of ultrasound, not only those involving the injection of microbubbles.

The use of NHP permitted to test the robustness of our system in detecting cavitation activity through highly heterogeneous conditions of ultrasound transmission. The real-time feedback control was capable of controlling the severity of disruption achieved by FUS; however, the evaluation of safety with MRI

precludes drawing conclusions on acute inflammatory responses or effects ~~on~~ the microstructure level of the brain tissue. A recent study has shown that FUS can induce a transient and controlled level of inflammation that can stimulate neurogenesis.[46] The use of small animal in statistically significant number of subjects can facilitate the exploration of our algorithm to achieve sufficient acoustic levels to induce neurogenesis while avoiding detrimental effects of chronic inflammation.

In summary, our system provides a large animal pre-clinical platform for brain disease models and treatment with relevant acoustic parameters for the clinical translation of non-invasive ultrasound-mediated BBB opening. Relative spectra of passive cavitation-based signals provided an optimum readout for the feedback control of the acoustic pressure, as well as ~~made possible~~ comparisons across animals and sessions. The feedback control of the acoustic pressure using relative PCD spectra is powerful mainly due to its system independence. Thus, other systems can benefit from this methodology after the calibration of the ~~ICD~~ ~~tolerated~~ (mainly dependent on system sensitivity).

Declaration of conflicting interests

The author(s) declared no potential conflicts of interest with respect to the research, authorship, and/or publication of this article

Authors' contributions

~~B L~~ and ~~P H~~ conceived and designed the study. HASK, JV, JF, and BL designed the experimental setup. HASK, JV, JF, RAB, and BL conducted the experiments with animals. HASK and BL designed the passive cavitation detection system and performed the calibrations. HASK, JF, AC, and BL performed data analysis. HASK wrote the manuscript. All authors reviewed the manuscript.

Supplementary material

Supplementary material for this paper can be found at the journal website: http://journals.sagepub.com/home/jcb.

References

1. Hammarlund-Udenaes M, de Lange ECM and Thorne RG (eds). *Drug delivery to the brain*. New York, NY: Springer, 2014.
2. Taylor EM. The impact of efflux transporters in the brain on the development of drugs for CNS disorders. *Clin Pharmacokinet* 2002; 41: 81–92.
3. Pardridge WM. The blood-brain barrier: bottleneck in brain drug development. *NeuroRx* 2005; 2: 3–14.
4. Escoffre J-M and Bouakaz A (eds). *Therapeutic ultrasound*. 1st ed. Cham: Springer International Publishing, 2016.
5. Banks WA. Characteristics of compounds that cross the blood-brain barrier. *BMC Neurol* 2009; 9: S3.
6. Hynynen K, McDannold N, Vykhodtseva N, et al. Noninvasive MR imaging-guided focal opening of the blood-brain barrier in rabbits. *Radiology* 2001; 220: 640–646.
7. Zhang Z, Xu K, Bi Y, et al. Low intensity ultrasound promotes the sensitivity of rat brain glioma to doxorubicin by down-regulating the expressions of P-glucoprotein and multidrug resistance protein 1 in vitro and in vivo. *PLoS One* 2013; 8: e70685.
8. Cho H, Lee H-Y, Han M, et al. Localized down-regulation of P-glycoprotein by focused ultrasound and microbubbles induced blood-brain barrier disruption in rat brain. *Sci Rep* 2016; 6: 31201.
9. Aryal M, Fischer K, Gentile C, et al. Effects on P-glycoprotein expression after blood-brain barrier disruption using focused ultrasound and microbubbles. *PLoS One* 2017; 12: e0166061.
10. Marty B, Larrat B, Van Landeghem M, et al. Dynamic study of blood–brain barrier closure after its disruption using ultrasound: a quantitative analysis. *J Cereb Blood Flow Metab* 2012; 32: 1948–1958.
11. Sun T, Samiotaki G, Wang S, et al. Acoustic cavitation-based monitoring of the reversibility and permeability of ultrasound-induced blood-brain barrier opening. *Phys Med Biol* 2015; 60: 9079–9094.
12. Kovacs ZI, Kim S, Jikaria N, et al. Disrupting the blood–brain barrier by focused ultrasound induces sterile inflammation. *Proc Natl Acad Sci U S A* 2017; 114: E75–E84.
13. Kinoshita M, McDannold N, Jolesz FA, et al. Noninvasive localized delivery of Herceptin to the mouse brain by MRI-guided focused ultrasound-induced blood-brain barrier disruption. *Proc Natl Acad Sci U S A* 2006; 103: 11719–11723.
14. Liu H-L, Hua M-Y, Chen P-Y, et al. Blood-brain barrier disruption with focused ultrasound enhances delivery of chemotherapeutic drugs for glioblastoma treatment. *Radiology* 2010; 255: 415–425.
15. Treat LH, McDannold N, Zhang Y, et al. Improved anti-tumor effect of liposomal doxorubicin after targeted blood-brain barrier disruption by MRI-guided focused

ultrasound in rat glioma. *Ultrasound Med Biol* 2012; 38: 1716–1725.

16. Raymond SB, Treat LH, Dewey JD, et al. Ultrasound enhanced delivery of molecular imaging and therapeutic agents in Alzheimer's disease mouse models. *PLoS One* 2008; 3: 1–7.

17. Jordão JF, Ayala-Grosso CA, Markham K, et al. Antibodies targeted to the brain with image-guided focused ultrasound reduces amyloid-?? Plaque load in the TgCRND8 mouse model of Alzheimer's disease. *PLoS One* 2010; 5: 4–11.

18. Baseri B, Choi JJ, Deffieux T, et al. Activation of signaling pathways following localized delivery of systemically administered neurotrophic factors across the blood-brain barrier using focused ultrasound and microbubbles. *Phys Med Biol* 2012; 57: N65–81.

19. Chen H, Yang GZX, Getachew H, et al. Focused ultrasound-enhanced intranasal brain delivery of brain-derived neurotrophic factor. *Sci Rep* 2016; 6: 28599.

20. Alonso A, Reinz E, Leuchs B, et al. Focal delivery of AAV2/1-transgenes into the rat brain by localized ultrasound-induced BBB opening. *Mol Ther Nucl Acids* 2013; 2: e73.

21. Wang S, Olumolade OO, Sun T, et al. Noninvasive, neuron-specific gene therapy can be facilitated by focused ultrasound and recombinant adeno-associated virus. *Gene Ther* 2015; 22: 104–110.

22. Burgess A, Ayala-Grosso CA, Ganguly M, et al. Targeted delivery of neural stem cells to the brain using MRI-guided focused ultrasound to disrupt the blood-brain barrier. *PLoS One* 2011; 6: e27877.

23. Deffieux T and Konofagou E. Numerical study of a simple transcranial focused ultrasound system applied to blood-brain barrier opening. *IEEE Trans Ultrason Ferroelectr Freq Control* 2010; 57: 2637–2653.

24. Kamimura HAS, Wang S, Wu S-Y, et al. Chirp- and random-based coded ultrasonic excitation for localized blood-brain barrier opening. *Phys Med Biol* 2015; 60: 7695–712.

25. Pinton G, Aubry J-F, Bossy E, et al. Attenuation, scattering, and absorption of ultrasound in the skull bone. *Med Phys* 2012; 39: 299–307.

26. McDannold N, Arvanitis CD, Vykhodtseva N, et al. Temporary disruption of the blood-brain barrier by use of ultrasound and microbubbles: safety and efficacy evaluation in rhesus macaques. *Cancer Res* 2012; 72: 3652–3663.

27. Downs ME, Buch A, Sierra C, et al. Long-term safety of repeated blood-brain barrier opening via focused ultrasound with microbubbles in non-human primates performing a cognitive task. *PLoS One* 2015; 10: 1–26.

28. Downs ME, Buch A, Karakatsani ME, et al. Blood-brain barrier opening in behaving non-human primates via focused ultrasound with systemically administered microbubbles. *Sci Rep* 2015; 5: 15076.

29. Wu S-Y, Sanchez CS, Samiotaki G, et al. Characterizing focused-ultrasound mediated drug delivery to the heterogeneous primate brain in vivo with acoustic monitoring. *Sci Rep* 2016; 6: 37094.

30. Marquet F, Tung YS, Teichert T, et al. Noninvasive, transient and selective blood-brain barrier opening in non-human primates in vivo. *PLoS One* 2011; 6: e22598.

31. Horodyckid C, Canney M, Vignot A, et al. Safe long-term repeated disruption of the blood-brain barrier using an implantable ultrasound device: a multiparametric study in a primate model. *J Neurosurg* 2017; 126: 1351–1361.

32. Carpentier A, Canney M, Vignot A, et al. Clinical trial of blood-brain barrier disruption by pulsed ultrasound. *Sci Transl Med* 2016; 8: 343re2.

33. Arvanitis CD, Livingstone MS and McDannold N. Combined ultrasound and MR imaging to guide focused ultrasound therapies in the brain. *Phys Med Biol* 2013; 58: 4749–4761.

34. Cline HE, Schenck JF, Hynynen K, et al. MR-guided focused ultrasound surgery. *J Comput Assist Tomogr* 1992; 16: [AQ1].

35. Magnin R, Rabusseau F, Salabartan F, et al. Magnetic resonance-guided motorized transcranial ultrasound system for blood-brain barrier permeabilization along arbitrary trajectories in rodents. *J Ther Ultrasound* 2015; 3: 1–11.

36. Mcdannold N, Vykhodtseva N and Hynynen K. Targeted disruption of the blood–brain barrier with focused ultrasound: association with cavitation activity. *Phys Med Biol Phys Med Biol* 2006; 51: 793–807.

37. Tung Y-S, Vlachos F, Choi JJ, et al. In vivo transcranial cavitation threshold detection during ultrasound-induced blood–brain barrier opening in mice. *Phys Med Biol* 2010; 55: 6141–6155.

38. O'Reilly MA and Hynynen K. Blood-brain barrier: real-time feedback-controlled focused ultrasound disruption by using an acoustic emissions-based controller. *Radiology* 2012; 263: 96–106.

39. Tsai C-H, Zhang J-W, Liao Y-Y, et al. Real-time monitoring of focused ultrasound blood-brain barrier opening via subharmonic acoustic emission detection: implementation of confocal dual-frequency piezoelectric transducers. *Phys Med Biol* 2016; 61: 2926–2946.

40. Sabraoui A, Inserra C, Gilles B, et al. Feedback loop process to control acoustic cavitation. *Ultrason Sonochem* 2011; 18: 589–594.

41. Hill CR, Bamber JC and Haar GR ter. *Physical principles of medical ultrasonics*, : . 2004,p. 511 [AQ2].

42. Arvanitis CD, Livingstone MS, Vykhodtseva N, et al. Controlled ultrasound-induced blood-brain barrier disruption using passive acoustic emissions monitoring. *PLoS One* 2012; 7: e45783.

43. Wu SY, Tung YS, Marquet F, et al. Transcranial cavitation detection in primates during blood-brain barrier opening-a performance assessment study. *IEEE Trans Ultrason Ferroelectr Freq Control* 2014; 61: 966–978.

44. Frigo M and Johnson SG. The design and implementation of FFTW3. *Proc IEEE* 2005; 93: 216–231.

45. Li H, Sun J, Zhang D, et al. Low-intensity (400 mW/cm^2, 500 kHz) pulsed transcranial ultrasound preconditioning may mitigate focal cerebral ischemia in rats. *Brain Stimul* 2017; 10: 695–702.

46. Mcmahon D, Bendayan R and Hynynen K. Acute effects of focused ultrasound-induced increases in blood-brain barrier permeability on rat microvascular transcriptome. *Sci Rep* 2017; 7: 1–15.